Pressure-induced disorder in Rb_2ZnCl_4

2009 J. Phys.: Condens. Matter 21 405405

(http://iopscience.iop.org/0953-8984/21/40/405405)

J. Phys.: Condens. Matter **21** (2009) 405405 (11pp) doi:10.1088/0953-8984/21/40/405405

Pressure-induced disorder in Rb_2ZnCl_4

Denis Machon[1], Andrzej Grzechnik[2] and Karen Friese[2]

[1] Université de Lyon, F-69000, France-Université de Lyon 1, Laboratoire PMCN, CNRS, UMR 5586, F-69622 Villeurbanne Cedex, France
[2] Departamento de Fisica de la Materia Condensada, Facultad de Cienca y Tecnologia, Universidad del Pais Vasco, Apartado 644, 48080 Bilbao, Spain

E-mail: denis.machon@lpmcn.univ-lyon1.fr

Received 16 June 2009, in final form 21 August 2009
Published 14 September 2009
Online at stacks.iop.org/JPhysCM/21/405405

Abstract
Rb_2ZnCl_4 in the normal phase ($T = 308$–313 K) has been studied under pressure by means of single-crystal x-ray diffraction up to 3.84 GPa and Raman spectroscopy up to 5.9 GPa. No pressure-induced phase transition has been observed but an orientational disorder of the tetrahedra is enhanced with the pressure. At the same time a partial one-dimensional correlation of some chlorine atoms might be favoured at high pressures. Raman spectra in the incommensurate phase ($T = 293$ K) were collected to higher pressure (24.2 GPa) varying the pressure-transmitting medium. The hydrostaticity during the compression is shown to affect drastically the broadness of the Raman peaks, leading to an amorphous-like spectrum in the least hydrostatic case.

1. Introduction

A_2BX_4 compounds with structures related to the β-K_2SO_4-type structure (space group $Pmcn$) have been the subject of many research works (see e.g. [1] and references therein), in particular as a template for studying incommensurate structure [2]. Among this family of compounds, Rb_2ZnCl_4 has been extensively studied as it undergoes a series of phase transformations as a function of temperature ([2, 3] and references therein). The orthorhombic, so-called normal phase (space group $Pmcn$ [4–6]), undergoes a phase transition to an incommensurate phase with a wavevector $q = [1/3 - \delta(T)]c^*$ at $T_i \approx 303$ K [2–4, 6–8]. This incommensurate structure transforms to a ferroelectric commensurate lock-in phase with a tripled c axis parameter at $T_L = 192$ K [2, 4, 8, 9]. For temperatures slightly above the lock-in transition a soliton regime has been described ([10] and references therein). A further phase transition to a monoclinic phase is observed at $T_3 = 72$ K [11, 12].

Rb_2ZnCl_4 has been studied under pressure and low temperature by means of dielectric and DTA measurements (up to about 0.8 GPa) [13], Brillouin spectroscopy (up to 0.6 GPa) [3], and acoustic methods (up to 0.4 GPa) [14]. It was found that the transition temperature T_i increases with increasing pressure at a rate of about 3.5–3.7 K GPa^{-1} [13, 14]. In addition, two new phases were discovered under pressure and at low temperature (figure 1). One of the phases (named phase IV) has a limited stability domain (~0.1–0.4 GPa and ~173–190 K). The second high-pressure phase (phase V) shows an extended domain of stability and is connected to the incommensurate phase, to the phase IV, and to the ferroelectric commensurate phase appearing below $T_2 = 192$ K at ambient pressure. These two high-pressure phases are of the improper ferroelastic type and a softening of two elastic modules is associated with these pressure-induced transitions [14]. Up to now, there has been no structural information available for these phases. The transition pressure between phase V and the incommensurate phase first increases with increasing temperature and should cross the normal–incommensurate transition line at about 1.1 GPa and 306 K. However, the transition line is curved and shows a plateau above 0.6 GPa and, thus, the transition temperature only slightly increases with pressure.

More recently, the study of the A_2BX_4 compound family under pressure led to a deeper understanding of the pressure-induced amorphization phenomenon [15–17]. The early work by Serghiou *et al* [18] concluded that only some of the A_2BX_4 compounds may amorphize with compression. The ratio BX_4/A (ratio of the size of the anionic BX_4 tetrahedral units to that of their interstitial A cation) seemed to allow discrimination between pressure-induced amorphization and pressure-induced crystal-to-crystal phase transitions. However, more recently, Machon *et al* demonstrated that the critical parameter was not the chemical composition but the local hydrostaticity provided during the compression [15, 17]. For instance, Cs_2HgBr_4 belongs to the A_2BX_4 compound family

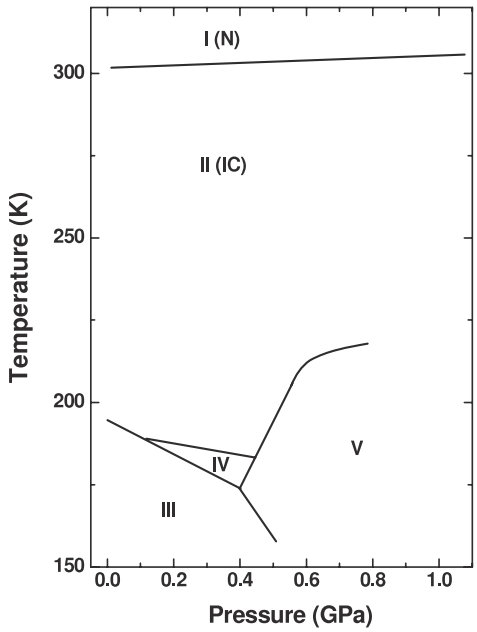

Figure 1. Pressure–temperature phase diagram of Rb_2ZnCl_4. Adapted from [13].

and has a ratio $BX_4/A = 1.563$, and should, according to [18], exhibit amorphization under pressure. During non-hydrostatic compression, an amorphous state was indeed observed using x-ray diffraction. However, when a quasi-hydrostatic pressure-transmitting medium was used, the amorphization was not complete [15]. A second experiment was even more illuminating. Using the same pressure-transmitting medium, we compare a compression on a powdered sample, on one hand, and a compression on a single crystal, on the other hand. In the experiment on the polycrystalline sample, a first phase transition prior to amorphization was detected, whereas the second experiment exhibited the following sequence of phase transitions: $Pnma$ ($Z = 4$) $\rightarrow$ incommensurate $\rightarrow$ $P2_1$, and no amorphous state was observed up to 20 GPa [15].

High-pressure studies on Rb_2ZnCl_4 are particularly interesting as the ratio $BX_4/A = 1.521$ lies at the threshold for which amorphization is expected according to [18]. Serghiou *et al* studied this compound under high pressure using energy-dispersive x-ray diffraction. Under compression providing the lowest degree of hydrostaticity (no pressure-transmitting medium), a transformation was observed between 1.1 and 10.9 GPa. With increasing pressure an amorphous feature appeared between 15.9 and 24.0 GPa and the pressure-induced amorphization was complete at 40 GPa. In another run, supposed to provide a more hydrostatic compression (argon as the pressure-transmitting medium but with the sample compacted as a pellet before loading into the diamond anvil cell), the first transformation was hardly observed but the amorphous state was achieved at pressure above 25.5 GPa. In both experiments the pressure-induced amorphization was reversible.

The aim of this paper is to report the high-pressure behaviour of Rb_2ZnCl_4 at comparatively low pressure ($P < 6$ GPa) under hydrostatic conditions in the normal ($T =$ 308–313 K) and in the incommensurate phase ($T = 293$ K). We are especially interested in investigating the possibility of a pressure-induced normal-to-incommensurate phase transition. The second aim of the present work is to investigate the relationship between hydrostaticity and the pressure-induced amorphization process in the A_2BX_4 family compounds at higher pressure.

2. Experimental details

The crystals of Rb_2ZnCl_4 studied here were previously investigated in [10].

Single-crystal x-ray data were measured using an Ahsbahs-type diamond anvil cell [19] at $T = 308$ K, using a Stoe diffractometer IPDS-2T with Mo Kα radiation. A 250 μm hole was drilled into a stainless steel gasket preindented to a thickness of about 120 μm. The intensities were indexed, integrated, and corrected for absorption using the STOE software[3]. Shaded areas of the images from the diamond anvil cell were masked prior to integration. The intensities were integrated simultaneously with three orientation matrices, corresponding to the crystal of Rb_2ZnCl_4 and to the two diamonds of the cell. Due to their hemispherical shape, no absorption correction was necessary for the diamond anvils. The ruby luminescence method [20] was used for pressure calibration and isopropanol, which is hydrostatic to 4.20 GPa [21] and does not react with Rb_2ZnCl_4, was used as a pressure-transmitting medium. Other pressure-transmitting media that are hydrostatic to higher pressures, e.g., various mixtures of methanol, ethanol, and water, dissolve our crystal. The data were refined using the program JANA2006 [22][4].

High-pressure Raman scattering experiments were carried out using two-membrane diamond anvil cells with low-fluorescence diamonds having the culet size of 700 μm and 350 μm, respectively. In a first experiment (with 700 μm culet diamonds), a randomly oriented single crystal was loaded and low-fluorescence paraffin oil was used as a nearly hydrostatic medium during pressurization experiments. A second experiment was carried out with the same configuration but at higher temperature ($T = 313$ K) using external heating. The temperature was controlled using a thermocouple fixed in the vicinity of the gasket.

Two other experiments were carried out at higher pressure (with 350 μm culet diamond) and ambient temperature with paraffin oil as the pressure-transmitting medium and with no pressure-transmitting medium, respectively. The powdered sample was loaded into a hole drilled in a stainless steel gasket. Several ruby chips were distributed throughout the sample chamber, and the pressures were determined using the ruby fluorescence method [20].

Raman spectra were obtained using a home-built high-throughput optical system based on Kaiser optical filters and an Acton 300i spectrograph with sensitive CCD detection.

[3] STOE & Cie GmbH, Darmstadt.

[4] Further details of the crystallographic investigations can be obtained from the Fachinformationszentrum Karlsruhe, D-76344 Eggenstein-Leopoldshafen, Germany, on quoting the depository number CSD 420930-420933.

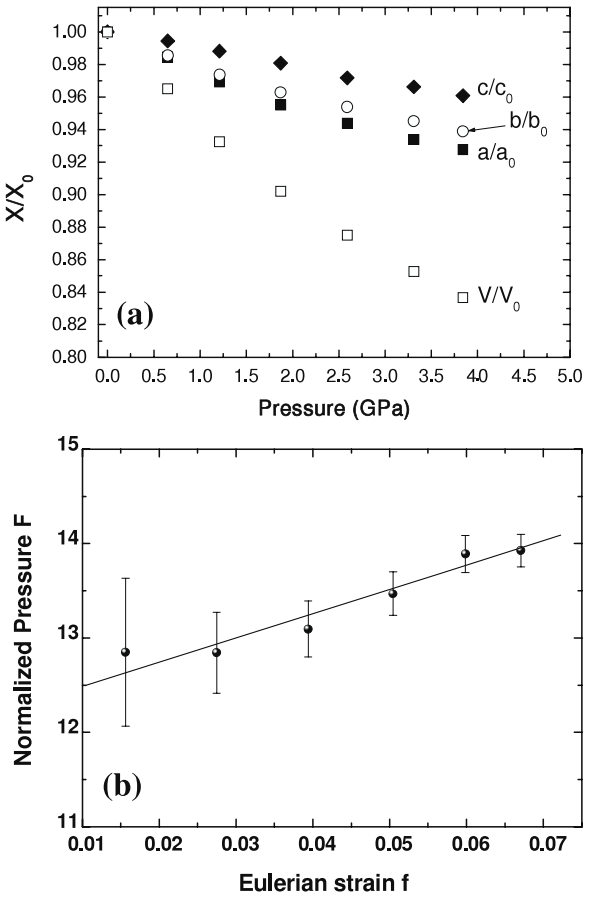

Figure 2. (a) Plot of the relative volume and the relative cell parameters with respect to ambient conditions X/X_0 for Rb_2ZnCl_4 as a function of pressure. (b) Plot of the normalized pressure (F) as a function of the Eulerian strain variable (f) for Rb_2ZnCl_4. $K_0 = 12.3(2)$ GPa and $K_0' = 5.3(2)$ were obtained from this reduced variable ($F - f$) plot.

Spectra were excited using 514.5 nm radiation from an air-cooled Ar^+ laser. The beam was focused onto the sample using a Mitutoyo 50× objective, with beam diameter ∼2 μm at the sample. The scattered light was collected in backscattering geometry using the same lens.

3. Results and discussion

3.1. X-ray diffraction at $T = 308$ K

The crystal structure of Rb_2ZnCl_4 ($Pmcn$, $Z = 4$) at ambient pressure above $T = 303$ K consists of isolated tetrahedra $ZnCl_4^{2-}$ and of two non-equivalent Rb^+ cations surrounded by nine and eleven chlorine atoms [4–6]. While in the first two investigations the ambient condition structure of Rb_2ZnCl_4 is described as perfectly ordered, Itoh *et al* [6] established a disordered model in which the chlorine atoms are moved away from the special position on the mirror plane perpendicular to the crystallographic a axis. They attributed the structural disorder to librational motions of the $ZnCl_4$ tetrahedra in two equivalent arrangements. Their conclusion was drawn from a comparison of single-crystal refinements in space group $Pmcn$ ($Z = 4$) assuming a *displacive* (=ordered) model isotypical to β-K_2SO_4 and an *order–disorder* model with all the Cl atoms at split positions, with the latter model being superior, according to the significance test developed by Hamilton [23]. Similar order–disorder phenomena were found in other representatives of the A_2BX_4 family of compounds [24, 25]. The disordered model as developed by Itoh *et al* was subsequently used to interpret the existence of additional Raman lines not predicted by group theory as will be discussed in the next section.

Table 1. Lattice parameters and unit-cell volumes as a function of pressure at $T = 308$ K ($Pmcn$, $Z = 4$).

P (GPa)	a (Å)	b (Å)	c (Å)	V (Å^3)
0.0001	7.281(2)	12.734(2)	9.235(3)	865.2
0.65	7.168(2)	12.550(2)	9.184(3)	826.2
1.21	7.057(2)	12.398(2)	9.126(3)	798.5
1.87	6.954(2)	12.260(2)	9.058(2)	772.2
2.59	6.873(2)	12.146(2)	8.974(3)	749.1
3.31	6.799(2)	12.036(2)	8.923(3)	730.2
3.84	6.753(2)	11.955(2)	8.873(3)	716.3

Indexing and analysis of our single-crystal x-ray diffraction data measured at 308 K indicated that the normal structure of Rb_2ZnCl_4 is stable upon compression to 3.84 GPa. A close inspection of the reconstructed reciprocal spaces for every data set did not reveal any reflections violating the extinction rules of space group $Pmcn$. No satellites were detected at any of the pressures suggesting that the normal → incommensurate transition was not crossed at this temperature.

Lattice parameters and unit-cell volumes are presented in figure 2(a) and table 1. The c axis is less compressible (linear compressibility $\beta_c = 1.0(1)$ GPa^{-1}) than the a and b axes (linear compressibilities $\beta_a = 1.9(1)$ GPa^{-1} and $\beta_b = 1.6(1)$ GPa^{-1}, respectively). The fitting procedure used here to obtained the bulk modulus (K_0) and its pressure derivative (K_0') involves transformation of the $V(P)$ data to the normalized or reduced stress–strain variables F and f. The Eulerian strain parameter (f) and the normalized pressure F are defined by

$$f = \frac{1}{2}\left[\left(\frac{V}{V_0}\right)^{-2/3} - 1\right] \tag{1}$$

$$F = P[3f(1+2f)^{2.5}]^{-1}. \tag{2}$$

This formalism yields the second-order finite strain equation

$$F = K_0[1 - 1.5(4 - K_0')f]. \tag{3}$$

We can then conduct a linear fit to the resulting $F(f)$ plot (figure 2(b)). In that case, well accepted goodness of fit criteria can be applied to the linear fit, and likely versus unlikely ranges of values for K_0' can be readily tested against the data within its error bars. K_0 and K_0' were then obtained as the intercept as $f \to 0$ and the slope of the $F(f)$ plot, respectively. This procedure yielded final values of $K_0 = 12.3(2)$ GPa and $K_0' = 5.3(2)$, for a measured $V_0 = 865.2$ Å^3.

In order to obtain more insight into the high-pressure behaviour of the commensurate structure of Rb_2ZnCl_4, we refined our data with the *displacive* and *order–disorder* models

Table 2. Experimental data for the single-crystal measurements at 0.65 and 3.84 GPa, $T = 308$ K ($Pmcn$, $Z = 4$).

	0.65 GPa	3.84 GPa
a (Å)	7.168(2)	6.753(2)
b (Å)	12.550(2)	11.955(2)
c (Å)	9.184(3)	8.873(3)
V (Å^3)	826.2	716.3
ρ (g cm^{-3})	3.039	3.505
μ (mm^{-1})	15.867	18.300
Range of hkl	$-7 \leqslant h \leqslant 6$	$-6 \leqslant h \leqslant 5$
	$-16 \leqslant k \leqslant 15$	$-15 \leqslant k \leqslant 13$
	$-10 \leqslant l \leqslant 11$	$-10 \leqslant l \leqslant 10$
No. measured refl.	3380	2639
No. unique refl.	683	367
No. observed refl.[a]	191	196
Redundancy	4.949	7.191
$R(\text{int})_{\text{obs/all}}$	12.43/16.72	13.27/13.35

[a] Criterion for observed reflections is $|F_{\text{obs}}| > 3\sigma$.

Table 3. Statistical factors for the refinements using the displacive and disordered models ($Pmcn$, $Z = 4$) at 0.65 and 3.84 GPa, $T = 308$ K. All agreement factors are given in %; weighting scheme $1/[\sigma^2(F_{\text{obs}}) + (0.01F_{\text{obs}})^2]$.

	Displacive model	*Order–disorder* model
0.65 GPa		
R_{obs}	12.21	11.52
wR_{obs}	9.58	8.96
GoF_{obs}	1.78	1.71
No. parameters	20	26
3.84 GPa		
R_{obs}	10.51	9.21
wR_{obs}	8.63	7.16
GoF_{obs}	2.25	2.03
No. parameters	20	26

taken from [6] at various pressures (tables 2–5). In each refinement, the thermal displacement parameters for all the atoms were treated isotropically.

Introducing Itoh's *order–disorder* model into the refinement of the ambient pressure data did not improve the fit. However, the results of the Hamilton test [23] clearly demonstrate that this model is becoming more and more superior to the *displacive* one on increasing pressure (table 3). This demonstrates that it is more important to take into account the disorder of the $ZnCl_4$ tetrahedra as the pressure is increased. The high-pressure behaviour thus seems to be analogous to that for increasing temperature at ambient pressure [6].

An analysis of the structural details that could be calculated from the parameters in tables 2, 4 and 5 reveals that the average Zn–Cl distance is independent of pressure. However, the $ZnCl_4$ tetrahedra do not behave as rigid units when exposed to pressure as the parameters describing the distortion of the tetrahedral are changing significantly with varying pressure. For example, the bond length distortion parameter (for the definition see [26]) is 1.378 at 0.69 GPa as compared to 0.797 at 3.84 GPa, indicating that the distribution of bond lengths gets more uniform at higher pressures. The coordination spheres around the Rb atoms are the most sensitive to pressure so their compression contributes the most

Table 4. Positional and isotropic thermal displacement parameters (in Å^2) in the *displacive* model ($Pmcn$, $Z = 4$) at 0.65 and 3.84 GPa, $T = 308$ K.

Atom	x	y	z	U_{iso}	Occ.
0.65 GPa					
Rb1	0.25	0.8210(5)	0.4825(6)	0.026(2)	1.0
Rb2	0.25	0.4038(6)	0.6300(8)	0.052(3)	1.0
Zn	0.25	0.4244(5)	0.2255(7)	0.016(2)	1.0
Cl1	0.25	0.414(2)	−0.014(2)	0.062(6)	1.0
Cl2	0.25	0.590(2)	0.321(2)	0.068(7)	1.0
Cl3	0.008(3)	0.342(1)	0.317(2)	0.067(5)	1.0
3.84 GPa					
Rb1	0.25	0.8295(6)	0.4818(7)	0.018(2)	1.0
Rb2	0.25	0.3959(6)	0.6235(8)	0.034(2)	1.0
Zn	0.25	0.4260(6)	0.2244(8)	0.013(2)	1.0
Cl1	0.25	0.407(1)	−0.023(2)	0.027(5)	1.0
Cl2	0.25	0.592(2)	0.323(2)	0.040(5)	1.0
Cl3	−0.012(4)	0.341(1)	0.320(2)	0.064(5)	1.0

Table 5. Positional and isotropic thermal displacement parameters (in Å^2) in the *order–disorder* model ($Pmcn$, $Z = 4$) at 0.65 and 3.84 GPa, $T = 308$ K.

Atom	x	y	z	U_{iso}	Occ.
0.65 GPa					
Rb1	0.25	0.6794(5)	0.5173(6)	0.029(2)	1.0
Rb2	0.25	0.4039(6)	0.8697(8)	0.053(2)	1.0
Zn	0.25	0.4243(5)	0.2746(6)	0.016(2)	1.0
Cl1	0.301(5)	0.415(1)	0.516(2)	0.034(6)	0.5
Cl2	0.213(8)	0.590(1)	0.181(2)	0.050(8)	0.5
Cl3	0.019(5)	0.322(2)	0.188(3)	0.038(8)	0.5
Cl4	0.504(6)	0.362(2)	0.177(3)	0.035(7)	0.5
3.84 GPa					
Rb1	0.25	0.6706(5)	0.5182(7)	0.022(2)	1.0
Rb2	0.25	0.3961(5)	0.8761(7)	0.033(2)	1.0
Zn	0.25	0.4258(5)	0.2759(7)	0.013(2)	1.0
Cl1	0.221(8)	0.408(1)	0.524(1)	0.018(6)	0.5
Cl2	0.211(7)	0.593(1)	0.177(2)	0.024(6)	0.5
Cl3	0.010(5)	0.315(2)	0.184(3)	0.027(7)	0.5
Cl4	0.536(5)	0.363(2)	0.176(2)	0.019(6)	0.5

to the bulk compressibility of Rb_2ZnCl_4. These observations suggest that all the materials with their structures related to the β-K_2SO_4 type have a common compressibility mechanism, regardless whether they are chlorides or oxides [27–29].

As mentioned above, the disordered model is clearly superior to the displacive model at high pressures. For the discussion of the pressure dependence of the disorder in the structure of Rb_2ZnCl_4 it is important to clarify first which of the chlorine positions in the disordered model can be combined to obtain $ZnCl_4$ tetrahedra of reasonable (or likely) geometry. Altogether eight chlorine positions are present in the disordered model: Cl1 to Cl4 with the coordinates given in table 5 and the position related via the mirror plane through symmetry operation $1/2 - x, y, z$. Following the nomenclature introduced by Itoh we will denote the first positions with primed and the second ones with double-primed symbols. At ambient pressure only two possible combinations of the chlorine positions yield reasonable tetrahedra: the combination I = [Cl1′ + Cl2′ + Cl3′ + Cl4′] and the combination II = [Cl1″ + Cl2″ + Cl3″ + Cl4″]. All

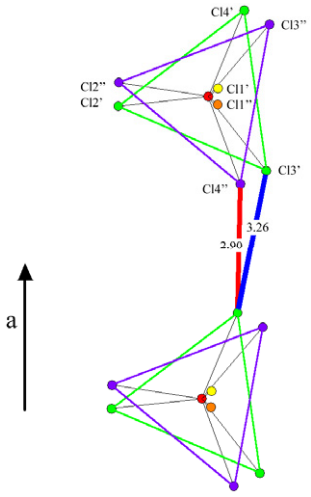

Figure 3. Partial view of the structure of Rb_2ZnCl_4 at 3.84 GPa along the *c* direction illustrating the arrangement of the different possible tetrahedral orientations in the structure. The two possible orientation of the basic planes of the tetrahedron (Cl2′ + Cl3′ + Cl4′ or Cl2″ + Cl3″ + Cl4″) are indicated by green and blue, respectively. For each basic plane two choices of the top chlorine atom (Cl1′ or Cl1″) are possible, resulting in four different combinations. Distances between neighbouring tetrahedra are indicated. The avoidance of the short Cl–Cl distance of 2.90 Å would result in a one-dimensional correlation of the basic planes of the tetrahedra.

(This figure is in colour only in the electronic version)

other combinations result in unreasonably close interatomic distances or large deviations from the tetrahedral angles. The shortest intratetrahedral Cl–Cl distance, assuming these two combinations as the only possibilities, is 3.45 Å, which corresponds exactly to the shortest possible intertetrahedral Cl–Cl distance assuming a random distribution of the differently oriented tetrahedra.

At 0.69 GPa this scenario is basically unchanged and again only two possible orientations are likely. The shortest intratetrahedral distance is now 3.50(5) Å and the tetrahedral angles for the combinations I and II range from 104.6(11)° to 116.3(7)°; the shortest intertetrahedral distance is 3.56(4) Å.

However, at 3.84 GPa the situation is substantially different. Four different combinations of atoms are now conceivable for obtaining tetrahedra: the two mentioned above and additionally the combination III = [Cl1″ + Cl2′ + Cl3′ + Cl4′] and the combination IV = [Cl1′ + Cl2″ + Cl3″ + Cl4″] (figure 3). This change is basically due to the fact that atoms Cl1′/Cl1″ are closer to the mirror plane perpendicular to the *a* axis when compared to their position at the lower pressures. The shortest intratetrahedral distance taking into account all four possible combinations is hardly changed as compared to the case for lower pressures (3.51(4) Å). The tetrahedral angles range from 104.4(6)–119.8(6)° (combination I and II) and 103.7(13)–118.4(7)° (the combinations III and IV). At 0.69 GPa the angular distortion would be considerably higher for the combinations III and IV (101.4(10)–121.5(11)°).

At 3.84 GPa, Cl–Cl distances involving neighbouring tetrahedra are considerably shortened and a number of them lie in the range from 3.2 to 3.3 Å. One individual distance Cl4′–Cl4″ between neighbouring tetrahedra deserves special attention as it is as short as 2.90(4) Å (figure 3). Even taking into account the fact that the pressure is high, this distance seems to be extremely small. If we assume that this short distance, which is parallel to the crystallographic *a* axis, is avoided within the structure this has a remarkable consequence: if we have one tetrahedron formed by the combinations I or III of chlorine atoms, i.e. containing Cl4′, the neighbouring tetrahedron in the *a* axis direction would also have to be a tetrahedron with Cl4′ (the combinations I or III), thus favouring the formation of the longer distance of 3.26 Å. This implies that the avoidance of this short distance would immediately result in a correlated arrangement of the basic planes of tetrahedra Cl4′–Cl2′–Cl3′ (or Cl4″–Cl2″–Cl3″) in the direction of the *a* axis, implying a partial one-dimensional correlation of some chlorine atoms in the structure (figure 3). However, neighbouring columns could still be uncorrelated in the *b*–*c* plane.

The effect of pressure on the degree of order in Rb_2ZnCl_4 could thus have two different consequences. On one hand, the disorder might be increased as the number of possible orientations of the tetrahedral is changed from 2 to 4, and, on the other hand, due to the fact that short Cl–Cl distances are probably avoided within the structure, partial one-dimensional chlorine correlations could be induced

An important observation to discuss is the absence of a transition to the incommensurate phase. The commensurate → incommensurate phase transition in Rb_2ZnCl_4 has been studied under high pressure using various techniques below 1 GPa [3, 13, 14]. The transition temperature increases with increasing pressure at a small rate of about 3.5–3.7 K GPa^{-1} [3, 13, 14]. Thus, at $T = 308$ K, the expected pressure of the transition should not exceed 1.5 GPa. The fact that we did not observe this transition indicates that the linear extrapolation is probably not valid and that there is a change in the pressure dependence of the critical temperature.

3.2. Raman spectroscopy at T = 313 K and 293 K

Raman spectra of Rb_2ZnCl_4 under pressure were recorded at two different temperatures ($T = 293$ K and $T = 313$ K) in two separate experiments. At $T = 293$ K Rb_2ZnCl_4 is in the incommensurate phase, while it is in the normal phase at $T = 313$ K.

Let us first discuss the results obtained in the normal phase and compare them with the x-ray diffraction data. The group theory analysis of the internal modes in the normal phase giving the correlation between the free ion tetrahedral symmetry and the symmetry of the normal phase D_{2h} through the site symmetry C_s has been presented in [30]. From this work, eight internal stretching Raman active modes (two modes associated with the ν_1 in-phase vibration and six modes associated with the ν_3 out-of-phase vibration) and ten internal bending modes (four modes associated with the ν_2 vibration and six modes associated with the ν_4 vibration) are expected. However, polarized Raman spectra obtained by Noiret *et al* [30] in the high-frequency (stretching) region showed that the actual number of observed bands is lower than predicted. This

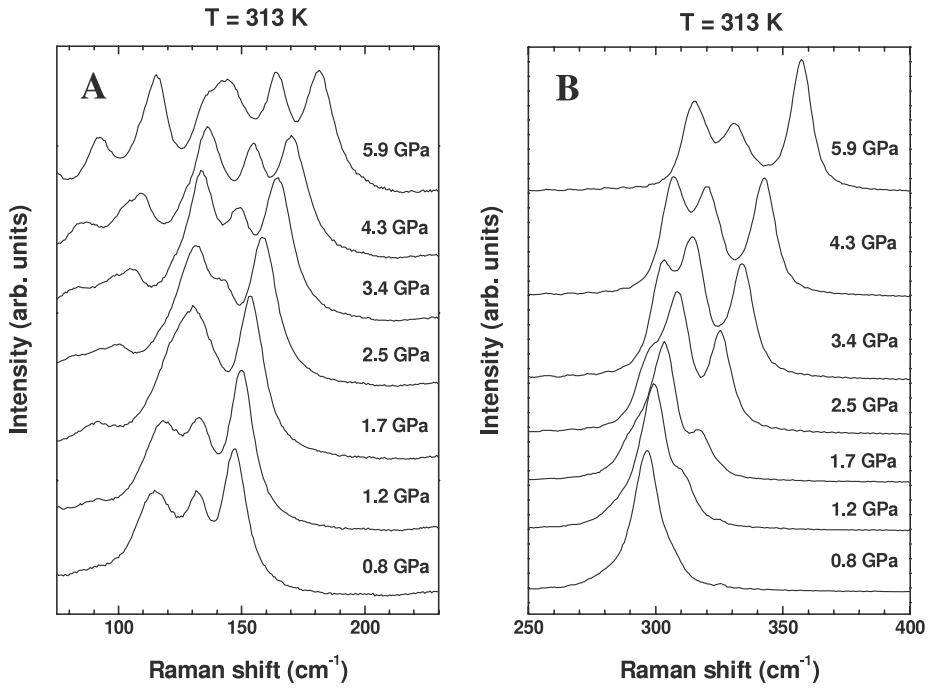

Figure 4. Evolution of the Raman spectra of a Rb_2ZnCl_4 single crystal in the normal phase with applied pressure between 0.8 and 5.9 GPa. (A) Bending internal modes. (B) Stretching internal modes.

indicates that the $(ZnCl_4)^{2-}$ ions interact weakly and only couple with the crystal. This leads only to a slight degeneracy removal of the vibrations. The two ν_1 vibrations expected (A_{1g} and B_{3g} symmetry) are measured at exactly the same position, 293.8 cm^{-1}. The ν_3 vibrations of the free ions should split into six components ($2A_g + 2B_{3g} + B_{1g} + B_{2g}$). Only five are observed, at 281.1 cm^{-1}(B_{3g}), 301.3 cm^{-1} (B_{1g}), 301.4 cm^{-1} (A_g), 302.0 cm^{-1} (B_{3g}) and 302.1 cm^{-1} (B_{2g}). In practice, only three modes could be observed, at 281.1, 293.8 and 301.7 cm^{-1} (average position of the four modes around this position). However, Noiret *et al* observed some additional peaks not predicted by the group theory analysis [30]. In (*ab*) and (*ac*) configurations (corresponding to the B_{1g} and B_{2g} symmetry, respectively), they observed four modes at 284.2 cm^{-1} (B_{2g}), 284.5 cm^{-1} (B_{1g}), 294.0 cm^{-1} (B_{2g}), and 294.1 cm^{-1} (B_{1g}). The authors interpreted the appearance of these extra modes as a consequence of the orientational disorder that may be present in the structure, as suggested by Itoh *et al* [6] and confirmed by numerical simulations [31, 32]. The main consequence of this disorder would be a breakdown of the selection rule validity for the ordered crystal and certain normally forbidden modes would be then allowed to appear. These extra modes are assigned as 'ungerade' modes becoming more or less weakly Raman active. In conclusion, the region of the spectrum corresponding to the stretching vibrations can be decomposed as follows: two ν_3 vibrations at 281.1 cm^{-1} and 301.7 cm^{-1}, one vibration at 284.3 cm^{-1} corresponding to the modes allowed by the disorder effect and a ν_1 component at 293.9 cm^{-1} mainly dominated by the A_g and B_{3g} allowed modes but also by two modes allowed by the disorder effect. No such assignment has been carried out for the bending modes region in Rb_2ZnCl_4.

Figure 4 shows the pressure-induced evolution of the Raman spectra of a non-oriented Rb_2ZnCl_4 single crystal up to 5.9 GPa. The Raman spectra were decomposed into individual Lorentzian components. Our fitting procedure was to start from the spectrum obtained at the highest pressure (here, $P = 5.9$ GPa) and to use the minimal number of components to obtain a satisfactory fit. The pressure evolution of the frequencies is given in figure 5. The peak positions of all the Raman bands are very sensitive to pressure and are shifted approximately linearly towards higher frequencies as pressure increases.

For the high-frequency range, we mainly observed a splitting into three main peaks. At first glance, we may think that this behaviour is simply a natural separation of the initially merged peaks due to their different pressure dependences. However, this explanation could not account for the changes in intensity of the peaks. As shown in figure 6, the intensity of the peaks at 288 and 306 cm^{-1} at ambient pressure continuously increases with the applied pressure. According to [30] the peak at around 288 cm^{-1} at ambient pressure is due to orientational disorder of the tetrahedron. According to the results from x-ray diffraction presented in the previous section, the number of possible orientations of the tetrahedron is increased at higher pressures from 2 to 4. This could explain the increase of the intensity of the peak at 288 cm^{-1} under pressure, in agreement with figure 6. The similar effect observed for the peak initially located at 306 cm^{-1} leads us to the conclusion that this peak is also due to an orientational disorder. Such an effect has already been observed in other molecular compounds such as $NaKSO_4$ and K_2CrO_4 for instance [27, 33]. The changes observed in the low-frequency region, especially the appearance of two peaks below 100 cm^{-1}, certainly results from the same disordering effect.

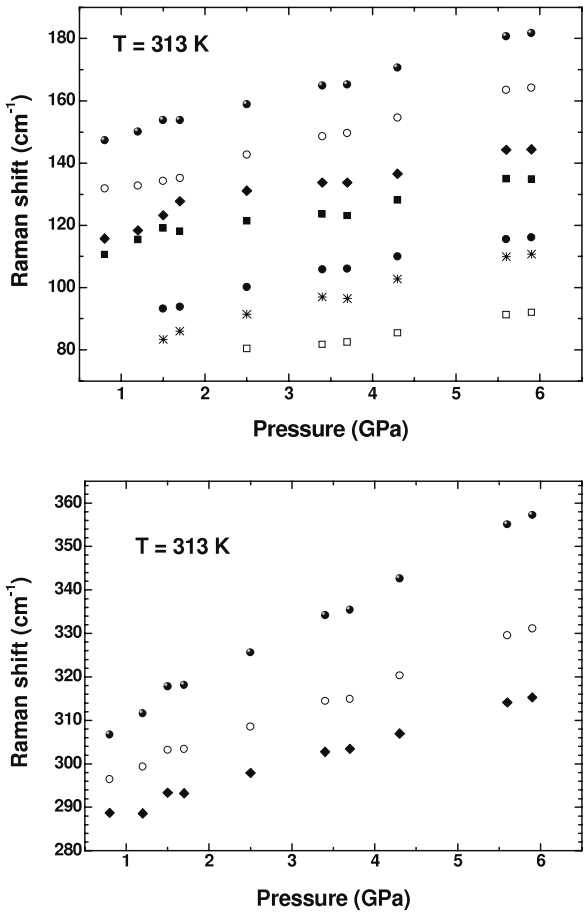

Figure 5. Pressure dependence of the (top) internal bending modes and (bottom) internal stretching modes in the $ZnCl_4$ tetrahedra in the normal phase.

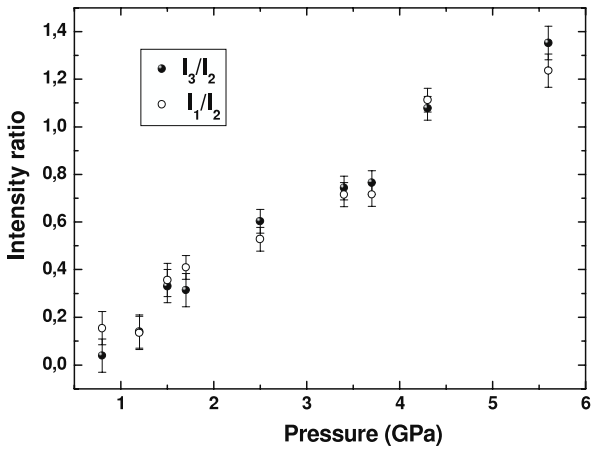

Figure 6. Pressure evolution of the ratios I_1/I_2 and I_3/I_2. I_1 and I_3 are the intensities of the peaks at 288 and 306 cm^{-1} at ambient pressure, respectively, and associated with the presence of some tetrahedral orientational disorder. I_2 is the intensity of the most intense peak at around 295 cm^{-1} at ambient pressure.

In conclusion, for the normal phase an orientational disordering of the tetrahedra is inferred from the presence of more lines in the region of the non-degenerate symmetric stretching mode of the $ZnCl_4$ ions than is permitted by group theoretical considerations for the crystal symmetry. X-ray diffraction experiments reported in the previous section fully support this pressure-induced disordering effect.

A second experiment was carried out at 293 K with a new loading of an unoriented single crystal in paraffin oil. Figure 7 shows the pressure-induced evolution of the Raman spectra up to 4.7 GPa. The evolution of the frequency is given in figure 8. Four components were used to fit the spectra up to 3.6 GPa, in agreement with the work of Noiret *et al* [30] that showed that an additional component appears in the stretching region when the crystal adopts the incommensurate structure. Otherwise, the high-pressure evolution is similar to what is observed in the normal phase.

The similarity of the pressure-induced evolutions in the normal phase and in the incommensurate phase leads us to conclude that the spectra in the incommensurate phase can be explained on the basis of a pressure-enhanced orientational disordering of the tetrahedra. Even though, to our knowledge, no disorder of the incommensurate phase was ever observed using diffraction methods, a link between the orientational disorder of the normal phase and that of the low-temperature phases has been underlined [30]. The orientational disorder in the normal phase would be connected with the modulation in the incommensurate phase which indicates a long-wavelength disorder of the tetrahedra. Thus, pressure appears as an interesting tool for achieving a better understanding of the nature of the incommensurate phase. In addition, the high-pressure evolution may be more complex, as observed for Rb_2ZnBr_4. For this related compound, it has been found that the pressure–temperature phase diagram is extremely rich, with several modulated commensurate and pseudo-commensurate phases [34–36]. Further x-ray diffraction or neutron diffraction study at high pressure for the incommensurate phase will help us to better understand phase transitions in these A_2BX_4 compounds and to include pressure as a parameter in a Landau model, for example [37].

At pressure above 3.6 GPa, a new peak is clearly observed at 353 cm^{-1}. This new peak may be due to a phase transition (to phase V) found at lower temperature in [13] (figure 1). However, it is not clear for the moment whether this peak indicates a phase transition or an effect on the positional modulation of the atoms. In addition, as shown in figure 9, the high-pressure changes are totally reversible.

3.3. The effect of hydrostaticity

In another set of experiments at $T = 293$ K, a study of the effect of hydrostaticity on the Raman spectra and the search for an amorphous phase has been undertaken. The first experiment consisting in the compression of a powdered Rb_2ZnCl_4 sample without any pressure-transmitting medium is shown on figure 10. The pressure evolution is rather similar to that in the previous experiment on a single crystal. Important changes in the spectra are observed above 12.3 GPa where a broadening of the spectrum, especially in the low-frequency region, is observed. These changes are in good agreement with the x-ray diffraction results published earlier where a

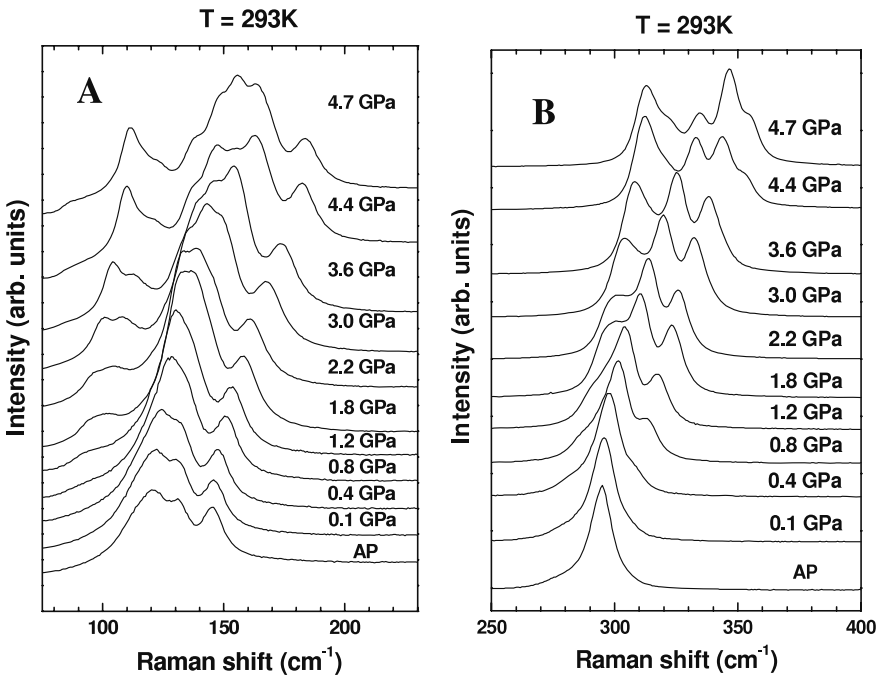

Figure 7. Evolution of the Raman spectra of a Rb_2ZnCl_4 single crystal in the incommensurate phase with applied pressure between ambient pressure (AP) and 4.7 GPa. (A) Bending internal modes. (B) Stretching internal modes.

phase transition has been observed in this pressure range [18]. The resulting spectrum at 15.8 GPa is surprising. It consists of two broad bands at 220 and 360 cm^{-1}. These features can be interpreted in terms of an amorphous compound obtained by pressurization, as observed for Cs_2HgBr_4 [15, 17]. However, an additional narrower peak is also observed at around 420 cm^{-1} and cannot be assigned to an amorphous feature. In addition, a narrow low-frequency peak at around 145 cm^{-1} is also observed at higher pressure.

These observations indicate that the sample is probably inhomogeneous, and that a crystalline phase coexists with an amorphous state. This is what has also been observed for Cs_2HgBr_4 [15, 17]. The appearance of an amorphous state instead of a crystalline phase in this latter compound has been demonstrated to be due to the local non-hydrostaticity experienced by the sample and has been interpreted in terms of the ferroelastic glass model [16, 17]. The second experiment where some paraffin oil has been used as the pressure-transmitting medium confirms this result (figure 11). In this case, the appearance of new peaks associated with some broadening starts at 11.3 GPa. With increasing pressure, the broadening increases. Amorphous-like spectra are obtained above 15 GPa. In this experiment, no sharp peak assigned to a crystalline phase could be observed. At a first glance, this result may be surprising as we may expect the paraffin oil to provide a better hydrostaticity and, thus, expect to observe stronger crystalline peaks and even to avoid the amorphous state. However, using the width of the ruby luminescence lines as a probe of the hydrostaticity as shown in figure 12, it clearly appears that the ruby chip experienced a better hydrostaticity surrounded by the Rb_2ZnCl_4 dry powder than when surrounded by paraffin oil. In the case of dry powder the part of the sample near the diamonds experienced a non-hydrostatic compression whereas the inside parts of the sample experienced a nearly hydrostatic compression due to the poor mechanical properties of Rb_2ZnCl_4. In the second configuration, paraffin oil provided a less hydrostatic compression for the whole sample leading to a complete amorphization of the sample. In addition, when the pressure is released, the Raman spectrum is identical to the one at ambient pressure before the pressurization experiment. Thus, the high-pressure transformations are totally reversible, again as observed for Cs_2HgBr_4 [15, 17], and in agreement with the previous x-ray diffraction data [18].

Two alternative scenarios may explain our observations, namely the appearance of amorphous-like spectra and the dependence of amorphization on non-hydrostaticity:

(a) an orientational disordering enhanced under pressure that may ultimately lead to a complete disordering of the structure resulting in an amorphous state as proposed in the case of pressure-induced amorphization of $LiKSO_4$ [38];
(b) the ferroelastic glass concept as proposed for the pressure-induced amorphization of the isostructural compound Cs_2HgBr_4.

The conditions for obtaining a ferroelastic glass are developed in [16] and can be summarized as follows: if we apply to a material close to a ferroelastic transition a non-hydrostatic compression corresponding to a stress field tensor involving shear stresses, it may either produce a crystalline phase with a stable crystalline configuration or cause the formation of a 'frustrated' multi-domain state, in which the different crystalline domains induced by the stress field tensor occur simultaneously. Structural mismatches between adjacent differently sheared domains then give rise to internal

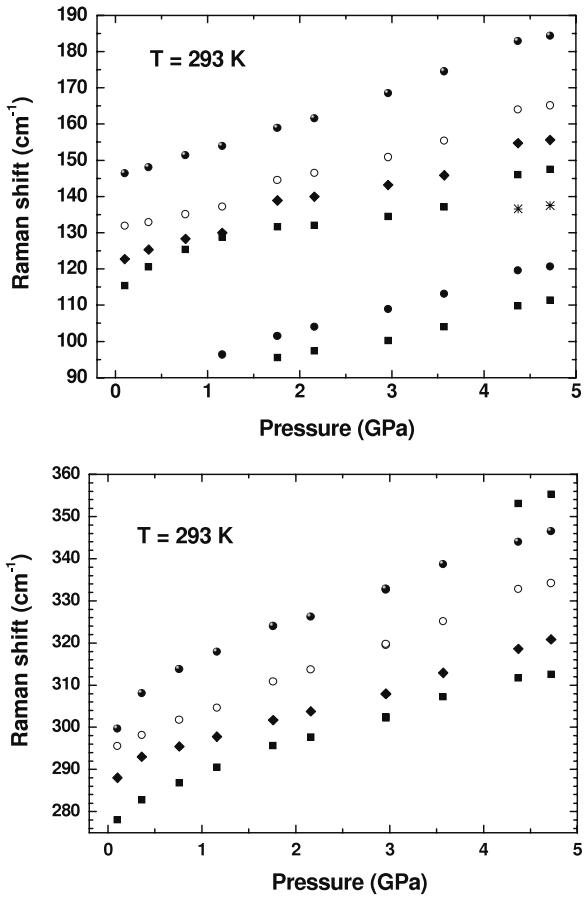

Figure 8. Pressure dependence of the (left) internal bending modes and (right) internal stretching modes in the $ZnCl_4$ tetrahedra. A new component appears between 3.6 and 4.2 GPa.

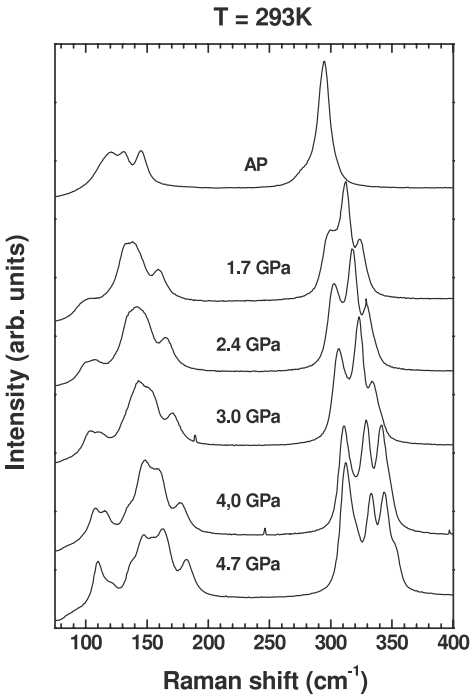

Figure 9. Raman spectra obtained during decompression from 4.7 GPa down to ambient pressure (AP). The pressure evolutions are reversible.

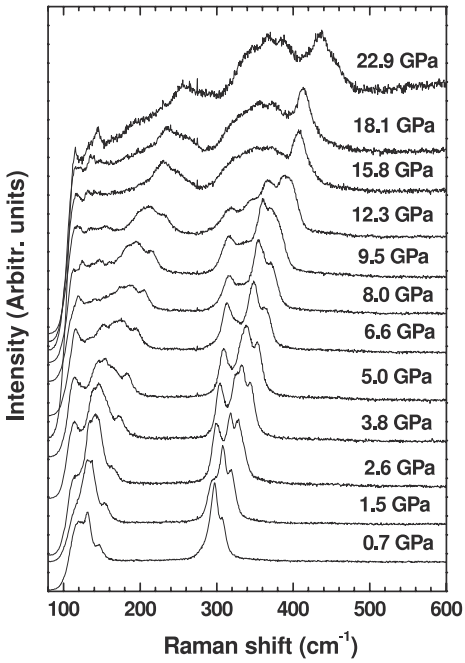

Figure 10. Evolution at 293 K of the Raman spectra of powdered Rb_2ZnCl_4 during compression without any pressure-transmitting medium.

stresses that produce a splitting of the mesoscopically sized domains and their progressive disintegration into ferroelastic nanodomains that appear at the length scale of x-ray diffraction experiments as a *glassy state*. Such a ferroelastic glass may form instead of its crystalline counterpart if (i) the ferroelastic phase exists in equivalent configurations corresponding to distinct spontaneous strain components, and (ii) an internal stress field is created in the sample which includes the stress components conjugated to the spontaneous strains.

A third scenario would combine (a) and (b). Bernardin and Hammack proposed that for related molecular compounds the orientational disorder would result from an impeded ferroelastic transition as stated in the ferroelastic glass model [33]. However, further experiments varying pressure, temperature and hydrostaticity (varying the pressure-transmitting medium and the crystal morphology, i.e., single crystal or powder) are required to conclude about the amorphization process.

4. Conclusions

X-ray diffraction and Raman spectroscopy data were obtained on Rb_2ZnCl_4 single crystals in the commensurate phase. No pressure-induced transition has been detected up to 5.9 GPa. However, both techniques confirm that an orientational disordering of the $ZnCl_4$ tetrahedra is enhanced with increasing pressure. At the same time, the x-ray data indicate that a one-dimensional column-like correlation of part of the chlorine atoms could take place in the structure.

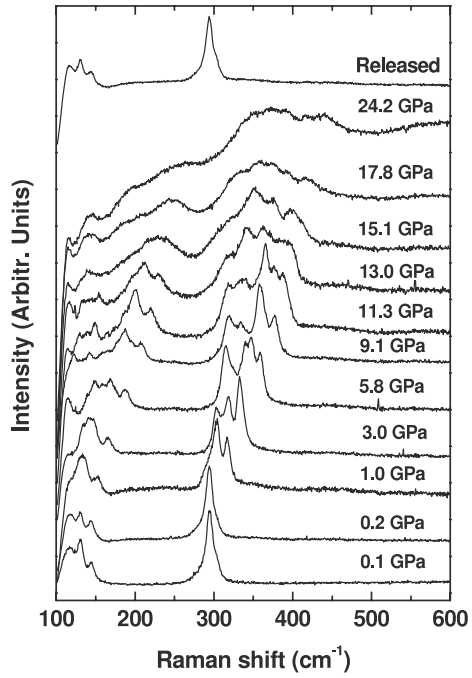

Figure 11. Evolution at 293 K of the Raman spectra of powdered Rb_2ZnCl_4 during compression with paraffin oil as the pressure-transmitting medium.

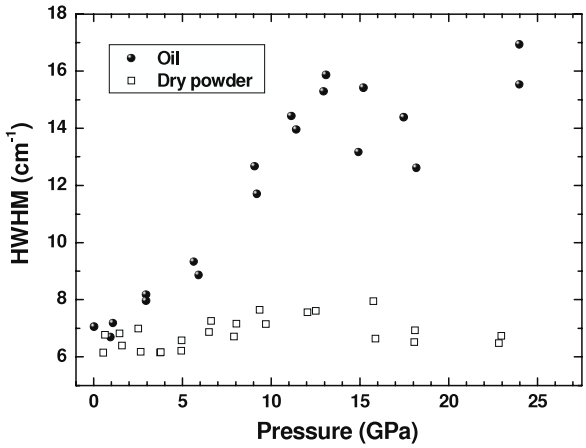

Figure 12. Half-width at half-maximum (HWHM) evolution of the luminescence ruby line in both experiments. Open squares: without any pressure-transmitting medium; circles: with oil as the pressure-transmitting medium.

Raman spectra of the incommensurate phase were obtained for Rb_2ZnCl_4 single crystals up to 4.7 GPa and for powdered samples up to 24.2 GPa. The results are similar to those for the normal phase, i.e., a pressure-enhanced orientational disorder, at least to 3.6 GPa. Above this pressure, a new stretching component is observed. It is not clear yet whether this component results from a pressure-induced phase transition or an effect on the positional modulation of the atoms. Under further non-hydrostatic compression, a strong broadening develops at pressure above around 10 GPa. An amorphous state is observed by Raman spectroscopy at 17.8 GPa in the least hydrostatic compression (paraffin oil as the pressure-transmitting medium) whereas a coexistence of an amorphous state and a crystalline phase is observed under more hydrostatic conditions.

Acknowledgments

We thank Dr Pierre Bouvier (Laboratoire des Matériaux et du Génie Physique, Institut National Polytechnique de Grenoble) for his comments. AG and KF acknowledge financial support by the Spanish Ministerio de Ciencia y Innovación (FIS2008-03834), the UPV and the Gobierno Vasco.

References

[1] Fabry J and Pérez-Mato J M 1994 *Phase Transit.* **49** 193
[2] Cummins H Z 1990 *Phys. Rep.* **185** 211
[3] Weishaupt K, Schmitz P J and Spatz J P 1995 *Solid State Commun.* **93** 177
[4] Quilichini M and Pannetier J 1983 *Acta Crystallogr.* B **39** 657
[5] Secco A S and Trotter J 1983 *Acta Crystallogr.* C **39** 317
[6] Itoh K, Hinasada A, Matsunaga H and Nakamura E 1983 *J. Phys. Soc. Japan* **52** 664
[7] Gutmann M J, Petricek V, Daoud-Aladine M A and Martin C Y 2008 *Meas. Sci. Technol.* **19** 034005–1
[8] Hedoux A, Grebille D, Jaud J and Godefroy G 1992 *Phase Transit.* **38** 127
[9] Parisi F and Bonadeo H 1997 *Acta Crystallogr.* A **53** 286
[10] Aramburu I, Friese K, Pérez-Mato J M, Morgenroth W, Aroyo M, Breczewski T and Madariaga G 2006 *Phys. Rev.* B **73** 014112
[11] Francke E, Le Postollec M, Mathieu J-P and Poulet H 1980 *Solid State Commun.* **33** 155
[12] Bagautdinov B S and Shekhtman V S 1999 *Physics Solid State* **41** 987
[13] Gesi K 1985 *Ferroelectrics* **64** 97
[14] Kityk A V, Soprunyuk V P and Vlokh O G 1993 *Phys. Status Solidi* a **138** 119
[15] Machon D, Dmitriev V P, Bouvier P, Timonin P N, Shirokov V and Weber H-P 2003 *Phys. Rev.* B **68** 144104
[16] Tolédano P and Machon D 2005 *Phys. Rev.* B **71** 024210
[17] Machon D, Bouvier P, Weber H-P and Tolédano P 2006 *J. Phys.: Condens. Matter* **18** 3443
[18] Serghiou G, Reichmann H-J and Boehler R 1997 *Phys. Rev.* B **55** 14765
[19] Ahsbahs H 1995 *Z. Kristallogr. Suppl.* **9** 42
Ahsbahs H 2004 *Z. Kristallogr.* **219** 305
[20] Piermarini G J, Block S, Barnett J D and Forman R A 1975 *J. Appl. Phys.* **46** 2774
Mao H K, Xu J and Bell P M 1986 *J. Geophys. Res.* **91** 4673
[21] Angel R J, Bujak M, Zhao J, Gatta G D and Jacobsen S D 2007 *J. Appl. Crystallogr.* **40** 26
[22] Petricek V, Dusek M and Palatinus L 2007 The crystallographic computing system *JANA2006* (Prague: Institute of Physics)
[23] Hamilton W C 1965 *Acta Crystallogr.* **18** 502
[24] Pinheiro C B, Jorio A, Pimenta M A and Speziali N L 1998 *Acta Crystallogr.* B **54** 197
[25] De Pater C J 1979 *Acta Crystallogr.* B **35** 299
[26] Renner B and Lehmann G 1986 *Z. Kristallogr.* **175** 53
[27] Edwards C M, Haines J, Butler I S and Léger J-M 1999 *J. Phys. Chem. Solids* **60** 529
[28] Serghiou G and Guillaume C 2004 *J. Solid State Chem.* **177** 4672
[29] Grzechnik A, Breczewski T and Friese K 2008 *J. Solid State Chem.* **181** 2914

[30] Noiret I, Guinet Y and Hedoux A 1995 *Phys. Rev.* B **52** 13206
[31] Edwardson P J, Katkanant V, Hardy J R and Boyer L L 1987 *Phys. Rev.* B **35** 8470
[32] Lu H M and Hardy J R 1992 *Phys. Rev.* B **45** 7609
[33] Bernardin F E and Hammack W S 1996 *Phys. Rev.* B **54** 7026
[34] Parlinski K, Currat R, Vettier C, Aleksandrova I P and Eckold G 1992 *Phys. Rev.* B **46** 106
[35] Shigematsu H, Kubota M, Nishi M, Mashiyama H and Matsui T 1999 *J. Phys. Soc. Japan* **68** 2679
[36] Asahi T and Hasebe K 2002 *J. Phys. Soc. Japan* **71** 2925
[37] Latković M, Bjeliš A and Dananić V 2000 *J. Phys.: Condens. Matter* **12** L293
[38] Arora A K and Sakuntala T 1992 *J. Phys.: Condens. Matter* **4** 8697